

Production of antimatter ${}^{5,6}\overline{\text{Li}}$ nuclei in central Au+Au collisions at $\sqrt{s_{NN}} = 200$ GeV

Kai-Jia Sun¹ and Lie-Wen Chen^{*1,2}

¹*Department of Physics and Astronomy and Shanghai Key Laboratory for Particle Physics and Cosmology, Shanghai Jiao Tong University, Shanghai 200240, China*

²*Center of Theoretical Nuclear Physics, National Laboratory of Heavy Ion Accelerator, Lanzhou 730000, China*

(Dated: November 11, 2021)

Combining the covariant coalescence model and a blast-wave-like analytical parametrization for (anti-)nucleon phase-space freezeout configuration, we explore light (anti-)nucleus production in central Au+Au collisions at $\sqrt{s_{NN}} = 200$ GeV. Using the nucleon freezeout configuration (denoted by FO1) determined from the measured spectra of protons (p), deuterons (d) and ${}^3\text{He}$, we find the predicted yield of ${}^4\text{He}$ is significantly smaller than the experimental data. We show this disagreement can be removed by using a nucleon freezeout configuration (denoted by FO2) in which the nucleons are assumed to freeze out earlier than those in FO1 to effectively consider the effect of large binding energy value of ${}^4\text{He}$. Assuming the binding energy effect also exists for the production of ${}^5\text{Li}$, ${}^5\overline{\text{Li}}$, ${}^6\text{Li}$ and ${}^6\overline{\text{Li}}$ due to their similar binding energy values as ${}^4\text{He}$, we find the yields of these heavier (anti-)nuclei can be enhanced by a factor of about one order, implying that although the stable (anti-) ${}^6\text{Li}$ nucleus is unlikely to be observed, the unstable (anti-) ${}^5\text{Li}$ nucleus could be produced in observable abundance in Au+Au collisions at $\sqrt{s_{NN}} = 200$ GeV where it may be identified through the p- ${}^4\text{He}$ ($\overline{\text{p}}\text{-}{}^4\overline{\text{He}}$) invariant mass spectrum. The future experimental measurement on (anti-) ${}^5\text{Li}$ would be very useful to understand the production mechanism of heavier antimatter.

PACS numbers: 25.75.-q, 25.75.Dw

I. INTRODUCTION

The quest for antimatter has become one of fundamental issues in contemporary physics, astronomy and cosmology since the discovery of the positron (the anti-electron) in cosmic radiation [1] which corresponds to the negative energy states of electrons predicted by Dirac [2]. Based on very general principles of relativistic quantum field theory, it is believed that each particle has its corresponding antiparticle of the same mass (but the opposite charge) and any physical system has an antimatter analog with an identical mass. Indeed, following the observation of antiprotons ($\overline{\text{p}}$) [3] and antineutrons ($\overline{\text{n}}$) [4], more complex antimatter nuclei such as antideuterons ($\overline{\text{d}}$) [5, 6], antihelium-3 (${}^3\overline{\text{He}}$) [7] and antitritons (${}^3\overline{\text{H}}$) [8] have been observed. In terrestrial laboratories, the antihydrogen atoms have also been produced [9] and can even survive for a long time in confinement [10]. Recently, STAR collaboration at RHIC reported the discovery of strange antimatter nucleus, the antihypertriton (${}^3_{\Lambda}\overline{\text{H}}$) [11], and the heavier antimatter nucleus antihelium-4 (${}^4\overline{\text{He}}$ or $\overline{\alpha}$) [12] in Au+Au collisions. The ALICE collaboration at LHC also claimed the observation of ${}^4\overline{\text{He}}$ in Pb+Pb collisions [13]. A recent review on antimatter production can be found in Ref. [14].

The study of antimatter nuclei production in heavy-ion collisions is of critical importance for a number of fundamental problems in physics, astronomy and cosmology. For example, the precision measurement of the mass difference between nuclei and anti-nuclei can test

the fundamental CPT theorem for systems bound by the strong interaction [20]. The measured production rate of light anti-nuclei in heavy-ion collisions provides a point of reference for possible future observations in cosmic radiation for the motivation of hunting for antimatter and dark matter in the Universe [16–19]. The antimatter nuclei production provides the possibility to test the interactions between antimatter and antimatter [20]. In addition, the production of light anti-nuclei in heavy-ion collisions can be used to extract the freezeout information of antinucleons in these collisions, which is useful to infer the properties of a new state of matter, i.e., quark-gluon plasma (QGP) possibly formed in these collisions as well as to understand how the QGP expands, cools and hadronizes, providing a new window (compared to the electromagnetic and hadronic probes) for exploring the dynamics of ultrarelativistic heavy-ion collisions.

The heaviest antimatter nucleus observed so far is ${}^4\overline{\text{He}}$, and it will remain the heaviest stable antimatter nucleus observed for the foreseeable future [12] barring some dramatic discoveries in space detectors due to some special production mechanism [21] or a new breakthrough in accelerator technology. This is because the (anti-)nucleus production rate in these heavy-ion collisions is found to reduce by a factor of about 10^3 for each additional (anti-)nucleon added to the (anti-)nucleus according to the measured yields of $\overline{\text{p}}$ (p), $\overline{\text{d}}$ (d), ${}^3\overline{\text{He}}$ (${}^3\text{He}$) and ${}^4\overline{\text{He}}$ (${}^4\text{He}$) [12], and thus the yield of the next heavier stable antimatter nucleus, antilithium-6 (${}^6\overline{\text{Li}}$), is expected to be down by a factor of about 10^6 compared to ${}^4\overline{\text{He}}$ assuming ${}^6\overline{\text{Li}}$ production rate follows the same exponential reduction law and is beyond the reach of current accelerator technology. However, a careful observation on the experimental yields of p ($\overline{\text{p}}$), d ($\overline{\text{d}}$), ${}^3\text{He}$ (${}^3\overline{\text{He}}$) and

*Corresponding author (email: lwchen@sjtu.edu.cn)

${}^4\text{He}$ (${}^4\overline{\text{He}}$) in central Au+Au collisions at $\sqrt{s_{NN}} = 200$ GeV from STAR [12] indicates that while the yields of p ($\overline{\text{p}}$), d ($\overline{\text{d}}$) and ${}^3\text{He}$ (${}^3\overline{\text{He}}$) follow an exponential reduction rate very well, the yield of ${}^4\text{He}$ (${}^4\overline{\text{He}}$) displays a significant enhancement (excess) compared to the exponential reduction rate. The coalescence model calculations also significantly underestimate the yield of ${}^4\text{He}$ (${}^4\overline{\text{He}}$) although they can successfully describe the yields of p ($\overline{\text{p}}$), d ($\overline{\text{d}}$) and ${}^3\text{He}$ (${}^3\overline{\text{He}}$) [22]. It is thus of great interest to understand the physics behind this enhancement for the yield of ${}^4\text{He}$ (${}^4\overline{\text{He}}$), which would be critically important for the future searching for heavier antimatter nuclei such as antilithium-5 (${}^5\overline{\text{Li}}$) and ${}^6\overline{\text{Li}}$ in heavy-ion collisions. In Ref. [21], the possibility of direct production of antimatter nuclei out of the highly correlated vacuum has been discussed, which provides a potentially more copious production mechanism for heavier antimatter nuclei in heavy-ion collisions.

In the present work, we propose that the enhancement of the ${}^4\text{He}$ (${}^4\overline{\text{He}}$) yield could be due to its large binding energy which leads to relatively earlier formation for ${}^4\text{He}$ (${}^4\overline{\text{He}}$) than for d ($\overline{\text{d}}$) and ${}^3\text{He}$ (${}^3\overline{\text{He}}$) in the heavy-ion collisions. Assuming the similar binding energy effects also exist for the production of ${}^5\text{Li}$, ${}^5\overline{\text{Li}}$, ${}^6\text{Li}$ and ${}^6\overline{\text{Li}}$, we find the predicted yields of these heavier (anti-)nuclei can be enhanced significantly, implying that although the stable (anti)- ${}^6\text{Li}$ nucleus is unlikely to be observed, the unstable (anti)- ${}^5\text{Li}$ nucleus could be produced in observable abundance in Au+Au collisions at RHIC.

II. THE THEORETICAL MODELS

Understanding particle production in heavy-ion collision at different energy regions is among the fundamental questions in nuclear and particle physics. Theoretically, the microscopic coalescence model [23–25] and the macroscopic thermal model [26–30] provide two important approaches to describe the light cluster production in heavy-ion collisions. In particular, these two approaches have been successfully applied recently to describe the production of light (anti-)nuclei in ultrarelativistic heavy-ion collisions at RHIC and LHC energies [22, 29–37]. In the present work, the theoretical formalism for the description of (anti-)nuclei production in heavy-ion collisions is based on the covariant coalescence model [38] together with the (anti-)nucleon phase-space freezeout configuration described by a blast-wave-like analytical parametrization [39] which has been shown to be very successful to describe the hadron phase-space freezeout configuration in ultrarelativistic heavy-ion collisions.

A. (Anti-)Nucleon phase-space freezeout configuration

One basic ingredient of the coalescence model is the emission source function, i.e., the phase-space freezeout

configuration, of the constituent particles. In principle, the phase-space freezeout configuration can be obtained dynamically from transport model simulations for heavy-ion collisions (see, e.g., Refs. [40–43]). In the present work, for simplicity, we describe the (anti-)nucleon phase-space freezeout configuration using a fireball-like model through a blast-wave-like analytical parametrization [39].

We assume that particles are emitted from a freezeout hypersurface Σ^μ where the particles are in local thermal equilibrium described by Lorentz invariant one-particle distribution function $f(x, p)$ given by [44]

$$f(x, p) = gh^{-3}[\exp((p^\mu u_\mu - \Omega)/kT) \pm 1]^{-1} \\ = g(2\pi)^{-3}[\exp(p^\mu u_\mu/kT)/\xi \pm 1]^{-1}, \quad (1)$$

where the reduced Planck constant $\hbar = \frac{h}{2\pi}$ is set to be 1, g is spin degeneracy factor, Ω is the chemical potential, $\xi = exp(\Omega/kT)$ is the fugacity which is directly related to particle number density, u_μ is the four-velocity of a fluid element in the fireball and T is the corresponding local temperature. For the phase-space freezeout configuration, instead of using the four coordinates (t, x, y, z) , it is convenient to use the cylindrical coordinates (τ, r, ϕ_s, η) (see, e.g., Ref. [45]) where $\tau = \sqrt{t^2 - z^2}$ is the longitudinal proper time, $\eta = \frac{1}{2} \ln(\frac{t+z}{t-z})$ is the longitudinal space-time rapidity, r is the transverse radius, and ϕ_s is the spatial azimuthal angle. Similarly, the four momentum (E, p_x, p_y, p_z) is transformed to (m_T, p_T, ϕ_p, y) where $p_T = \sqrt{p_x^2 + p_y^2}$ is the transverse momentum, $y = \frac{1}{2} \ln(\frac{E+p_z}{E-p_z})$ is rapidity, $m_T = \sqrt{m^2 + p_T^2}$ is transverse mass, and ϕ_p is the azimuthal angle in momentum space. The four coordinate and momentum can thus be expressed as $x^\mu = (\tau \cosh \eta, r \cos \phi_s, r \sin \phi_s, \tau \sinh \eta)$ and $p^\mu = (m_T \cosh y, p_T \cos \phi_p, p_T \sin \phi_p, m_T \sinh y)$, respectively.

The one-particle invariant momentum distribution can be obtained as

$$E \frac{d^3 N}{dp^3} = \frac{d^3 N}{p_T dp_T dy d\phi_p} = \int_{\Sigma^\mu} d^3 \sigma_\mu p^\mu f(x, p), \quad (2)$$

with $dp^3 = E p_T dp_T dy d\phi_p$. For the particle production at midrapidity in heavy-ion collisions that we are considering in this work, we adopt the longitudinal boost invariance assumption [46]. By setting the longitudinal flow velocity $\nu_L = z/t$, the longitudinal flow rapidity $\eta_{flow} = \frac{1}{2} \ln[(1 + \nu_L)/(1 - \nu_L)]$ will be identical to the space-time rapidity $\eta = \frac{1}{2} \ln[(t+z)/(t-z)]$, and thus the four-velocity can be expressed as

$$u^\mu = \cosh \rho(r, \phi_s) (\cosh \eta, \tanh \rho(r, \phi_s) \cos \phi_b, \\ \tanh \rho(r, \phi_s) \sin \phi_b, \sinh \eta), \quad (3)$$

where ρ is the transverse rapidity of a fluid element in the fireball. The above expression can be obtained by a longitudinal boost with velocity $\tanh \eta$ multiplied by a transverse boost with velocity $\tanh \rho$ [39]. If we fix the

freezeout hypersurface Σ^μ by choosing a constant proper time τ , i.e., Σ^μ is independent of the transverse coordinates, then the covariant normal vector can be expressed as

$$d^3\sigma_\mu = (\cosh(\eta), 0, 0, -\sinh(\eta))\tau r dr d\eta d\phi_s. \quad (4)$$

Therefore, one can obtain

$$\begin{aligned} p^\mu u_\mu &= m_T \cosh \rho \cosh(\eta - y) - p_T \sinh \rho \cos(\phi_p - \phi_b), \\ p^\mu d^3\sigma_\mu &= \tau m_T \cosh(\eta - y) d\eta r dr d\phi_s, \end{aligned} \quad (5)$$

where ϕ_b is azimuthal direction of the transverse flow [39]. Considering that the freezeout can happen in some time interval, a Gaussian distribution for the freezeout proper time is introduced as follows

$$J(\tau) = \frac{1}{\Delta\tau\sqrt{2\pi}} \exp\left(-\frac{(\tau - \tau_0)^2}{2(\Delta\tau)^2}\right), \quad (6)$$

which satisfies

$$\int J(\tau) d\tau = 1, \quad \int \tau J(\tau) d\tau = \tau_0,$$

where τ_0 is the mean value of τ and $\Delta\tau$ is the dispersion of the τ distribution function. Therefore, the momentum distribution can be obtained as

$$\frac{d^3N}{p_T dp_T dy d\phi_p} = \int_{\Sigma^\mu} m_T \cosh(\eta - y) f(x, p) J(\tau) \tau d\tau d\eta r dr d\phi_s. \quad (7)$$

Following Ref. [39], we parameterize the transverse rapidity of a fluid element in the fireball as

$$\rho = \rho_0 \tilde{r} [1 + \epsilon \cos(2\phi_b)], \quad (8)$$

where ρ_0 is the isotropic part of the transverse flow, ϵ is the anisotropic part, ϕ_b is azimuthal direction of the transverse flow which is not identical to spatial azimuthal angle ϕ_s , and \tilde{r} is the ‘‘normalized elliptical radius’’

$$\tilde{r} = \sqrt{\frac{[r \cos \phi_s]^2}{R_x^2} + \frac{[r \sin \phi_s]^2}{R_y^2}}, \quad (9)$$

with

$$\tan \phi_s = \left(\frac{R_y}{R_x}\right)^2 \tan \phi_b, \quad (10)$$

where $R_x = R_0(1 + s_2)$ is the minor axis of the ellipse, $R_y = R_0(1 - s_2)$ is the major axis, and s_2 is the geometric anisotropy. Therefore, the transverse rapidity can also be written as

$$\rho = \rho_0 \sqrt{\frac{[r \cos \phi_s]^2}{R_x^2} + \frac{[r \sin \phi_s]^2}{R_y^2}} [1 + \epsilon \cos 2\phi_b]. \quad (11)$$

For midrapidity region ($y = 0$) in central heavy-ion collisions that we are considering here, one has $s_2 = \epsilon = 0$

and $\phi_b = \phi_s$, and thus the invariant distribution function can be expressed as

$$f(x, p) = \frac{g}{(2\pi)^3} \left[\exp\left(\frac{(m_T \cosh \rho \cosh(\eta) - p_T \sinh \rho \cos(\phi_p - \phi_s))/kT}{\xi \pm 1}\right) \right]^{-1} \quad (12)$$

with $\rho = \rho_0 r/R_0$. One can thus use formula (7) and (12) to calculate transverse momentum distribution of midrapidity particles in central heavy-ion collision.

B. Covariant coalescence model

In this work, we calculate light (anti-)nucleus production in ultrarelativistic heavy-ion collisions using the covariant coalescence formalism [38]. In the coalescence model, the probability for producing a nucleus is determined by the overlap of its Wigner phase-space density with the nucleon phase-space distribution at freezeout. We consider that M nucleons are combined to form one nucleus and the total multiplicity of the nucleus can be obtained as

$$\begin{aligned} N_c &= g_c \int \left(\prod_{i=1}^M dN_i \right) \rho_c^W(x_1, \dots, x_M; p_1, \dots, p_M) \\ &= g_c \int \left(\prod_{i=1}^M d\tau_i J(\tau_i) p_i^\mu d^3\sigma_{i\mu} \frac{d^3p_i}{E_i} f(x_i, p_i) \right) \times \\ &\quad \rho_c^W(x_1, \dots, x_M; p_1, \dots, p_M), \end{aligned} \quad (13)$$

where $\rho_c^W(x_1, \dots, x_M; p_1, \dots, p_M)$ is the Wigner density function which gives the coalescence probability, g_c is the coalescence factor [24]. By inserting δ function to conserve momentum, the invariant differential transverse momentum distribution of the nucleus becomes

$$\begin{aligned} E \frac{d^3N_c}{d^3P} &= E g_c \int \left(\prod_{i=1}^M d\tau_i J(\tau_i) p_i^\mu d^3\sigma_{i\mu} \frac{d^3p_i}{E_i} f(x_i, p_i) \right) \times \\ &\quad \rho_c^W(x_1, \dots, x_M; p_1, \dots, p_M) \delta^3(\mathbf{P} - \sum_{i=1}^M \mathbf{p}_i). \end{aligned} \quad (14)$$

The above formula is Lorentz invariant [38] and the Wigner function is a Lorentz scalar.

For the Wigner function $\rho_c^W(x_1, \dots, x_M; p_1, \dots, p_M)$, following Ref. [40, 42], instead of calculating it directly using four dimensional coordinators x_i and four dimensional momenta p_i of the constituent nucleons, we calculate it in the rest frame of the nucleus. To do so, a Lorentz transformation is performed to obtain the space-time and energy-momentum coordinates of each nucleon in the rest frame of the nucleus. To determine the spatial coordinates of the nucleons at equal time in the rest frame of the nucleus, i.e., $\mathbf{r}_1, \mathbf{r}_2, \dots, \mathbf{r}_M$, the nucleons that freeze out earlier are allowed to propagate freely with

constant velocity given by the ratio of their momentum and energies in the rest frame of the nucleus, until the time when the last nucleons in the nucleus freezes out. Furthermore, in order to calculate the Wigner function, Jacobi coordinate is adopted by a transformation of the coordinate as follows [40–42, 47]

$$\begin{pmatrix} \mathbf{R} \\ \mathbf{q}_1 \\ \vdots \\ \mathbf{q}_{M-1} \end{pmatrix} = J_M \begin{pmatrix} \mathbf{r}_1 \\ \mathbf{r}_2 \\ \vdots \\ \mathbf{r}_M \end{pmatrix}, \quad (15)$$

where $\mathbf{R} = \frac{\sum_{j=1}^M m_j \mathbf{r}_j}{\sum_{j=1}^M m_j}$ is the center-of-mass position vector of the nucleus and $\mathbf{q}_i = \sqrt{\frac{i}{i+1}} \left(\frac{\sum_{j=1}^i m_j \mathbf{r}_j}{\sum_{j=1}^i m_j} - \mathbf{r}_{i+1} \right)$ is the relative coordinate vector. Correspondingly, in the momentum space, one has

$$\begin{pmatrix} \mathbf{P} \\ \mathbf{k}_1 \\ \vdots \\ \mathbf{k}_{M-1} \end{pmatrix} = (J_M^{-1})^T \begin{pmatrix} \mathbf{p}_1 \\ \mathbf{p}_2 \\ \vdots \\ \mathbf{p}_M \end{pmatrix}, \quad (16)$$

where \mathbf{P} is the total momentum of the nucleus and \mathbf{k}_i is the relative momentum vector. The determinant of the Jacobi matrix is $|J_M| = 1/\sqrt{M}$, and one then has the following identity

$$\prod_{i=1}^M d^3 x_i d^3 p_i = d^3 R d^3 P \prod_{i=1}^{M-1} d^3 q_i d^3 k_i. \quad (17)$$

Furthermore, we assume the harmonic wave function for all the light (anti-)nuclei in the rest frame except the (anti-)deutrons for which we use the well-known Hulthén wave function (see, e.g., Refs. [40, 41]). The Wigner function of the nucleus can then be obtained as [42]

$$\begin{aligned} & \rho_c^W(x_1, \dots, x_M; p_1, \dots, p_M) \\ &= \rho^W(q_1, \dots, q_{M-1}, k_1, \dots, k_{M-1}) \\ &= 8^{M-1} \exp \left[- \sum_{i=1}^{M-1} (q_i^2 / \sigma_i^2 + \sigma_i^2 k_i^2) \right], \end{aligned} \quad (18)$$

with $\sigma_i^2 = (m_i \omega)^{-1}$ where the harmonic oscillator frequency ω is related to the root-mean-square (rms) radius of the nucleus as follows

$$\langle r_M^2 \rangle = \frac{3}{2M} \frac{1/\omega}{\sum_{i=1}^M m_i} \sum_{i=1}^M \left[m_i \left(\sum_{j=i+1}^M \frac{1}{m_j} + \sum_{j=1}^{i-1} \frac{1}{m_j} \right) \right] \quad (19)$$

Therefore, σ_i^2 can be determined by $\langle r_M^2 \rangle$. In the case of $m_1 = m_2 = \dots = m_M = m$, one can obtain $\sigma^2 = \frac{2M}{3(M-1)} \langle r_M^2 \rangle$.

TABLE I: Parameters of the blast-wave-like analytical parametrization for (anti-)nucleon phase-space freezeout configuration.

	T(MeV)	ρ_0	R_0 (fm)	τ_0 (fm/c)	$\Delta\tau$ (fm/c)	ξ_p	$\xi_{\bar{p}}$
FO1	111.6	0.98	15.6	10.55	3.5	10.45	7.84
FO2	111.6	0.98	12.3	8.3	3.5	21.4	16.04

III. RESULT AND DISCUSSION

A. (Anti-)Nucleon freezeout configuration from light (anti-)nuclei production

We focus on the midrapidity light (anti-)nuclei production in central Au+Au collisions at $\sqrt{s_{NN}} = 200$ GeV in this work. In this case, there are totally six parameters in the blast-wave-like analytical parametrization for (anti-)nucleon phase-space freezeout configuration, namely, the kinetic freeze-out temperature T , the transverse rapidity ρ_0 , the longitudinal mean proper time τ_0 , the time dispersion $\Delta\tau$, the transverse size at freeze-out R_0 , and the fugacity of particle ξ .

For proton phase-space freezeout configuration, we obtain the local temperature $T = 111.6$ MeV, the transverse rapidity $\rho_0 = 0.978$, and a constraint on the combination of the proton fugacity ξ_p , τ_0 , $\Delta\tau$ and R_0 , by fitting the measured spectrum of protons in Au+Au collisions at $\sqrt{s_{NN}} = 200$ GeV for 0-5% centrality [48]. To extract the values of ξ_p , τ_0 , $\Delta\tau$ and R_0 , we further fit the measured spectra of deuterons and ^3He [49] simultaneously using the results from the coalescence model (see the Subsection III B for the details), which leads to $R_0 = 15.6$ fm, $\tau_0 = 10.55$ fm/c, $\Delta\tau = 3.5$ fm/c and $\xi_p = 10.45$. For antiprotons, we assume they have the same phase-space freezeout configuration as protons except the fugacity is reduced to $\xi_{\bar{p}} = 7.84$ to describe the measured yield ratio $\bar{p}/p = 0.75$ [48]. Table I summarizes the parameters of the blast-wave-like analytical parametrization for (anti-)nucleon phase-space freezeout configuration (denoted as FO1). It should be pointed out that we have neglected the difference between protons and neutrons (antiprotons and antineutrons) for the phase-space freezeout configuration due to the small isospin chemical potential at freezeout in Au+Au collisions at $\sqrt{s_{NN}} = 200$ GeV [29]. Based on the freezeout configuration of (anti-)nucleons, one can then predict the production of light (anti-)nuclei using the coalescence model.

B. The production of light (anti-)nuclei

We use the coalescence model described above to calculate the production of light (anti-)nuclei. In the coalescence model, the statistical factor g_c is quite important and it is given by $g_c = \frac{2j+1}{2^N}$ [24] with j and N being, respectively, the spin and the nucleon number of the nu-

TABLE II: Statistical factor g_c , root-mean-square radii r_{rms} [50, 51] and binding energy E_b [52] of light (anti-)nuclei

	d (\bar{d})	${}^3\text{He}$ (${}^3\overline{\text{He}}$)	${}^4\text{He}$ (${}^4\overline{\text{He}}$)	${}^5\text{Li}$ (${}^5\overline{\text{Li}}$)	${}^6\text{Li}$ (${}^6\overline{\text{Li}}$)
g_c	$\frac{(2 \times 1 + 1)}{2^2}$	$\frac{(2 \times \frac{3}{2} + 1)}{2^3}$	$\frac{(2 \times 0 + 1)}{2^4}$	$\frac{(2 \times \frac{3}{2} + 1)}{2^5}$	$\frac{(2 \times 1 + 1)}{2^6}$
r_{rms} (fm)	1.96	1.76	1.45	2.5	2.5
E_b (MeV)	2.224	7.718	28.296	26.330	31.994

cleus. The spins of d, ${}^3\text{He}$, ${}^4\text{He}$, ${}^5\text{Li}$ and ${}^6\text{Li}$ are 1, 1/2, 0, 3/2 and 1, respectively. Furthermore, the rms radius r_{rms} of the light nucleus is also important since it determines the harmonic oscillator frequency parameter ω in the Wigner function of the nucleus. The r_{rms} of d, ${}^3\text{He}$, ${}^4\text{He}$, ${}^5\text{Li}$ and ${}^6\text{Li}$ are taken to be 1.96 fm, 1.76 fm, 1.45 fm, 2.5 fm and 2.5 fm, respectively [50, 51]. Here the $r_{\text{rms}} = 2.5$ fm for ${}^5\text{Li}$ is estimated based on the work in Ref. [51]. For the antinuclei, we assume they have the same ground state properties as their corresponding nuclei. Table II summarizes the statistical factors, rms radii as well as the binding energies [52] of different light (anti-)nuclei. It should be mentioned that while d (\bar{d}), ${}^3\text{He}$ (${}^3\overline{\text{He}}$), ${}^4\text{He}$ (${}^4\overline{\text{He}}$) and ${}^6\text{Li}$ (${}^6\overline{\text{Li}}$) are stable, ${}^5\text{Li}$ (${}^5\overline{\text{Li}}$) is unstable against the proton (antiproton) decay with half-life of about 370×10^{-24} s (i.e., 111 fm/c) [53] and thus it may be identified through the p- ${}^4\text{He}$ (\bar{p} - ${}^4\overline{\text{He}}$) invariant mass spectrum in heavy-ion collisions.

Figure 1 shows the predicted midrapidity transverse momentum distributions of p, d, ${}^3\text{He}$, ${}^4\text{He}$, ${}^5\text{Li}$ and ${}^6\text{Li}$ together with the experimental data of p from PHENIX collaboration [48] and the data of p, d, ${}^3\text{He}$ and ${}^4\text{He}$ from STAR collaboration [12, 49, 54] in central Au+Au collisions at $\sqrt{s_{NN}} = 200$ GeV. It is seen that the coalescence model predictions with the freezeout configuration FO1 are in very good agreement with the measured transverse momentum distributions of p, d and ${}^3\text{He}$ as expected but significantly underestimate the measured yield of ${}^4\text{He}$ by a factor of about 6. The similar feature was also observed in the calculations in Ref. [22].

From Table II, one can see that ${}^4\text{He}$ has a specially larger binding energy value compared to d or ${}^3\text{He}$, and thus it is more tightly bound and could be formed in relatively earlier stage in heavy-ion collisions compared to d or ${}^3\text{He}$. Physically, the light nuclei can be formed in principle in the whole dynamical process of heavy-ion collisions, but they are usually destroyed immediately after their formation due to the violating collisions in the high temperature environment. However, for the light nuclei with large binding energy values such as ${}^4\text{He}$, the survival probability in relatively earlier stage in heavy-ion collisions is expected to enhance compared to the loosely bound d and ${}^3\text{He}$. In principle, these effects can be studied using transport model simulations with dynamic light cluster production in heavy-ion collisions [55] although this is highly nontrivial and beyond the scope of this work. In the present work, to effectively mimic this binding energy effect, we assume the volume (time)

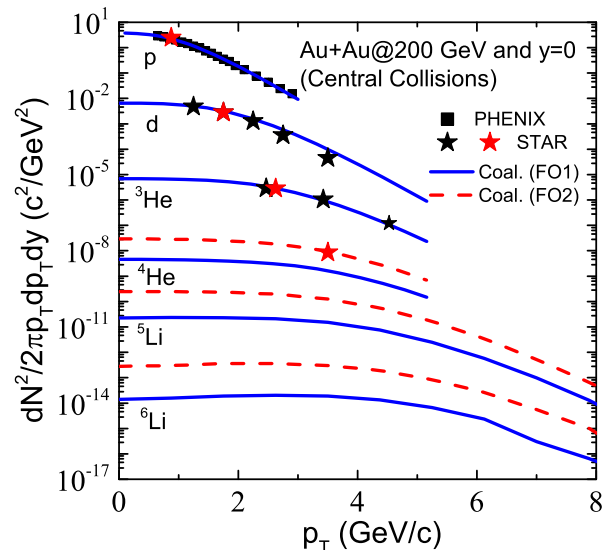


FIG. 1: Transverse momentum distributions of light nuclei at midrapidity ($y=0$) in central Au+Au collisions at $\sqrt{s_{NN}} = 200$ GeV predicted by coalescence model with FO1 (solid lines) and FO2 (dashed lines). The experiment data of protons is taken from the PHENIX measurement [48] whereas those of light nuclei are from the STAR measurement [12, 49]. The data point of protons from STAR measurement has been scaled by a factor of 0.6 to correct the weak decay effects [54].

of the freezeout hypersurface for nucleons coalesced into ${}^4\text{He}$ is smaller (shorter) than that of d or ${}^3\text{He}$. For simplicity, we reduce R and τ by a factor 1.27 to fit the measured yield of ${}^4\text{He}$, and this leads to $R = 12.3$ fm, $\tau = 8.3$ fm/c, $\Delta\tau = 3.5$ fm/c and $\xi_p = 21.4$, which is denoted as the phase-space freezeout configuration FO2 and is summarized in Table I. Since the binding energy values of ${}^5\text{Li}$ and ${}^6\text{Li}$ are also large and comparable with that of ${}^4\text{He}$ as shown in Table II, it is thus expected that the nucleons coalesced into ${}^5\text{Li}$ and ${}^6\text{Li}$ should have similar phase-space freezeout configuration as those coalesced into ${}^4\text{He}$. In Fig. 1, we also include the predicted transverse momentum distributions of ${}^4\text{He}$, ${}^5\text{Li}$ and ${}^6\text{Li}$ with the freezeout configuration FO2. It is seen that using the freezeout configuration FO2 significantly enhance the yields of ${}^5\text{Li}$ and ${}^6\text{Li}$ by a factor of about 9 and 16, respectively, compared to the case using FO1.

Figure 2 shows the differential invariant yields ($d^2N/(2\pi p_T dp_T dy)$) of (anti-)nuclei evaluated at the transverse momentum $p_T/|B| = 0.875$ GeV/c as a function of baryon number B . One can see that the coalescence model with FO1 reproduces the measured differential invariant yields of p (\bar{p}), d (\bar{d}) and ${}^3\text{He}$ (${}^3\overline{\text{He}}$) very well but significantly underestimates the measured value of ${}^4\text{He}$ (${}^4\overline{\text{He}}$), as already observed in Fig. 1. The dashed lines in Fig. 2 are obtained by fitting the differential invariant yields of p (\bar{p}), d (\bar{d}) and ${}^3\text{He}$ (${}^3\overline{\text{He}}$) by using an exponential function $e^{-r|B|}$. It is seen that the differential invariant yields of p (\bar{p}), d (\bar{d}) and ${}^3\text{He}$ (${}^3\overline{\text{He}}$)

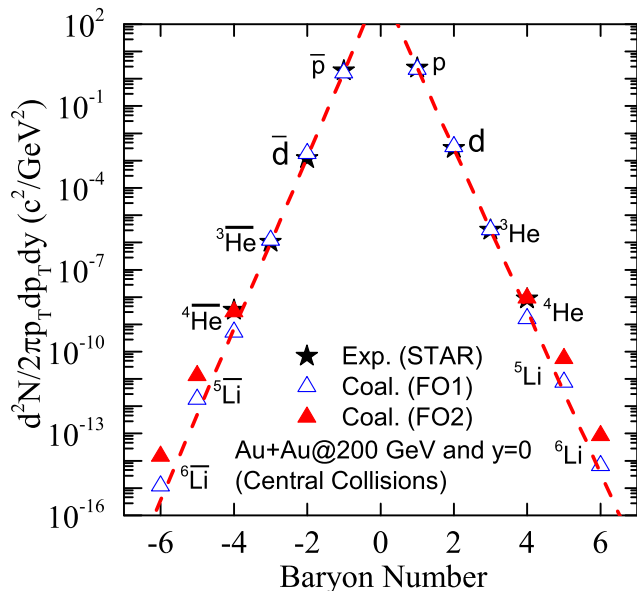


FIG. 2: The differential invariant yields $d^2N/(2\pi p_T dp_T dy)$ of (anti-)nucleus at the transverse momentum $p_T/|B| = 0.875$ GeV/c as a function of baryon number B in central Au+Au collisions at $\sqrt{s_{NN}} = 200$ GeV. The solid (open) triangles represent the coalescence model predictions with FO1 (FO2). The data point of protons from STAR measurement has been scaled by a factor of 0.6 to correct the weak decay effects [54].

follow the exponential function very well, depicting the same exponential reduction rate of the differential invariant yields with the increased atomic mass number for p (\bar{p}), d (\bar{d}) and ${}^3\text{He}$ (${}^3\bar{\text{He}}$). For ${}^4\text{He}$ (${}^4\bar{\text{He}}$), however, the measured differential invariant yields significantly deviate from the exponential function although the coalescence model prediction with FO1 still follows the same exponential reduction rate. For ${}^5\text{Li}$ (${}^5\bar{\text{Li}}$) and ${}^6\text{Li}$ (${}^6\bar{\text{Li}}$), the predicted differential invariant yields with FO1 deviate the exponential reduction rate by an enhancement factor of about 2.25 (3.57) and 1.87 (3.31) whereas those with FO2 display a much stronger enhancement by a factor of about 16.6 (26.3) and 23.3 (41.2), respectively, indicating a very strong binding energy effect.

Table III lists the p_T -integrated yield in the midrapidity region ($-0.5 \leq y \leq 0.5$), i.e., dN/dy at $y = 0$, of light (anti-)nuclei. One can easily obtain the midrapidity yield ratios d/p (\bar{d}/\bar{p}) = 4.65×10^{-3} (3.47×10^{-3}) and ${}^3\text{He}/d$ (${}^3\bar{\text{He}}/\bar{d}$) = 1.99×10^{-3} (1.50×10^{-3}). In particular, if we take the midrapidity yield of ${}^4\text{He}$ (${}^4\bar{\text{He}}$) as the value predicted by the coalescence model with FO2, we find the midrapidity yield ratios of ${}^5\text{Li}/{}^4\text{He}$ (${}^5\bar{\text{Li}}/{}^4\bar{\text{He}}$) and ${}^6\text{Li}/{}^4\text{He}$ (${}^6\bar{\text{Li}}/{}^4\bar{\text{He}}$) increase, respectively, from 1.32×10^{-3} (0.99×10^{-3}) and 1.67×10^{-6} (0.94×10^{-6}) with FO1 to 11.7×10^{-3} (8.74×10^{-3}) and 26.4×10^{-6} (14.9×10^{-6}) with FO2. These results indicate that the binding energy effects can enhance the midrapidity yields of ${}^5\text{Li}$ (${}^5\bar{\text{Li}}$) and ${}^6\text{Li}$ (${}^6\bar{\text{Li}}$) by a factor of about 8.77 (8.82) and 15.9 (15.8), respectively.

TABLE III: p_T -integrated yield in the mid-rapidity ($-0.5 \leq y \leq 0.5$) of light (anti-)nuclei.

	p	d	${}^3\text{He}$	${}^4\text{He}$	${}^5\text{Li}$	${}^6\text{Li}$
FO1	16.1	7.49E-02	1.49E-04	1.54E-07	1.22E-09	1.53E-12
FO2	16.1	-	-	9.18E-07	1.07E-8	2.43E-11
	\bar{p}	\bar{d}	${}^3\bar{\text{He}}$	${}^4\bar{\text{He}}$	${}^5\bar{\text{Li}}$	${}^6\bar{\text{Li}}$
FO1	12.1	4.21E-02	6.29E-05	4.88E-08	2.88E-10	2.73E-13
FO2	12.1	-	-	2.91E-07	2.54E-09	4.32E-12

IV. CONCLUSION

Based on the covariant coalescence model with a blast-wave-like analytical parametrization for the (anti-)nucleon phase-space freezeout configuration, we have extracted (anti-)nucleon freezeout information in central Au+Au collisions at $\sqrt{s_{NN}} = 200$ GeV by fitting the measured spectra of protons, deuterons and ${}^3\text{He}$. We have found that the covariant coalescence model with the obtained (anti-)nucleon phase-space freezeout configuration significantly underestimates the measured yield of ${}^4\text{He}$ (${}^4\bar{\text{He}}$). We have shown the predicted ${}^4\text{He}$ yield can be enhanced to the measured value by using a nucleon freezeout configuration in which the nucleons are assumed to freeze out earlier than those coalesced into deuterons and ${}^3\text{He}$ to effectively consider the large binding energy value of ${}^4\text{He}$. The similar conclusion has been obtained for ${}^4\bar{\text{He}}$.

Assuming the similar binding energy effect also exists for the production of heavier (anti-) ${}^5\text{Li}$ and (anti-) ${}^6\text{Li}$ due to their comparable binding energy values with ${}^4\text{He}$, we have predicted the spectra and yields of (anti-) ${}^5\text{Li}$ and (anti-) ${}^6\text{Li}$ in central Au+Au collisions at $\sqrt{s_{NN}} = 200$ GeV. Our results indicate that the binding energy effect can significantly enhance the yields of (anti-) ${}^5\text{Li}$ and (anti-) ${}^6\text{Li}$. In particular, the midrapidity yield ratios ${}^5\text{Li}/{}^4\text{He}$ (${}^5\bar{\text{Li}}/{}^4\bar{\text{He}}$) and ${}^6\text{Li}/{}^4\text{He}$ (${}^6\bar{\text{Li}}/{}^4\bar{\text{He}}$) increase, respectively, from 1.32×10^{-3} (0.99×10^{-3}) and 1.67×10^{-6} (0.94×10^{-6}) without binding energy effects to 11.7×10^{-3} (8.74×10^{-3}) and 26.4×10^{-6} (14.9×10^{-6}) with binding energy effects. Our results imply that although the stable (anti-) ${}^6\text{Li}$ nucleus is unlikely to be observed, the unstable (anti-) ${}^5\text{Li}$ nucleus could be produced in observable abundance in ultrarelativistic heavy-ion collisions at RHIC where it may be identified through the p - ${}^4\text{He}$ (\bar{p} - ${}^4\bar{\text{He}}$) invariant mass spectrum.

Our present study suggests that the future experimental measurement on the production of (anti-) ${}^5\text{Li}$ in central Au+Au collisions at $\sqrt{s_{NN}} = 200$ GeV would be extremely useful to test the binding energy effect on the light (anti-)nuclei production, and thus to understand the production mechanism of heavier antimatter nuclei in ultrarelativistic heavy-ion collisions, especially the observed enhancement for the yield of ${}^4\text{He}$ (${}^4\bar{\text{He}}$) compared to those of p (\bar{p}), d (\bar{d}) and ${}^3\text{He}$ (${}^3\bar{\text{He}}$). Any deviation of the measured (anti-) ${}^5\text{Li}$ yield in central Au+Au collisions

at $\sqrt{s_{NN}} = 200$ GeV from the coalescence model prediction with or without considering the binding energy effect may indicate the exist of new excitation mechanism, e.g., the direct production of nuclei out of the highly correlated vacuum.

Acknowledgments

We are grateful to Che Ming Ko, Yu-Gang Ma and Zhang-Bu Xu for helpful discussions. This work was sup-

ported in part by the Major State Basic Research Development Program (973 Program) in China under Contract Nos. 2015CB856904 and 2013CB834405, the NNSF of China under Grant Nos. 11275125 and 11135011, the ‘‘Shu Guang’’ project supported by Shanghai Municipal Education Commission and Shanghai Education Development Foundation, the Program for Professor of Special Appointment (Eastern Scholar) at Shanghai Institutions of Higher Learning, and the Science and Technology Commission of Shanghai Municipality (11DZ2260700).

-
- [1] C. D. Anderson, *Phys. Rev.* **43**, 491 (1933).
 [2] P. A. M. Dirac, *Proc. R. Soc. Lond. A* **117**, 610 (1928).
 [3] O. Chamberlain, E. Segre, C. Wiegand, and T. Ypsilantis, *Phys. Rev.* **100**, 947 (1955).
 [4] B. Cork, G. R. Lambertson, O. Piccioni, and W. A. Wenzel, *Phys. Rev.* **104**, 1193 (1956).
 [5] T. Massam, T. Muller, B. Righini, M. Schneegans, and A. Zichichi, *Nuovo Cim.* **39**, 10 (1965).
 [6] D. E. Dorfan, J. Eades, L. M. Lederman, W. Lee, and C. C. Ting, *Phys. Rev. Lett.* **14**, 1003 (1965).
 [7] Y. M. Antipov et al., *Yad. Fiz.* **12**, 311 (1970).
 [8] N. K. Vishnevsky et al., *Yad. Fiz.* **20**, 694 (1974).
 [9] G. Baur et al., *Phys. Lett.* **B368**, 251 (1996).
 [10] G. B. Andresen et al. (ALPHA Collaboration), *Nature Phys.* **7**, 558 (2011).
 [11] B. I. Abelev et al. (The STAR Collaboration), *Science* **328**, 58 (2010).
 [12] B. I. Abelev et al. (The STAR Collaboration), *Nature* **473**, 353 (2011).
 [13] N. Sharma, *J. Phys. G* **38**, 124189 (2011).
 [14] Y. G. Ma, J. H. Chen, and L. Xue, *Front. Phys.* **7**, 637 (2012); *Y. G. Ma, J. Phys.: Conf. Series* **420**, 012036 (2013); *EPJ Web of Conf.* **66**, 04020 (2014).
 [15] J. Adam et al. (ALICE Collaboration), *Nature Phys.*, (2015). DOI: 10.1038/NPHYS3432.
 [16] S. Ahlen et al., *Nucl. Instrum. Methods* **A350**, 351 (1994).
 [17] H. Fuke et al., *Phys. Rev. Lett.* **95**, 081101 (2005).
 [18] F. Donato, N. Fornengo, and D. Maurin, *Phys. Rev. D* **78**, 043506 (2008).
 [19] K. Abe et al., *Phys. Rev. Lett.* **108**, 131301 (2012).
 [20] L. Adamczyk et al. (The STAR Collaboration), *Nature*, in press, (2015) [arXiv:1507.07158].
 [21] W. Greiner, *Int. J. Mod. Phys. E* **5**, 1 (1996); *J. Phys.: Conf. Series* **413**, 012002 (2013).
 [22] L. Xue, Y. G. Ma, J. H. Chen, and S. Zhang, *Phys. Rev. C* **85**, 064912 (2012).
 [23] S. T. Butler and C. A. Pearson, *Phys. Rev. Lett.* **7**, 69 (1961).
 [24] H. Sato and K. Yazaki, *Phys. Lett.* **B98**, 153 (1981).
 [25] L. P. Csernai and J. I. Kapusta, *Phys. Rep.* **131**, 223 (1986).
 [26] J. Cleymans, K. Redlich, and E. Suhonen, *Z. Phys. C* **51**, 137 (1991).
 [27] F. Becattini and U. W. Heinz, *Z. Phys. C* **76**, 269 (1997).
 [28] P. Braun-Munzinger and J. Stachel, *Nature* **448**, 302 (2007).
 [29] A. Andronic, P. Braun-Munzinger, J. Stachel, and H. Stoecker, *Phys. Lett.* **B697**, 203 (2011).
 [30] J. Cleymans, S. Kabana, I. Kraus, H. Oeschler, K. Redlich, and N. Sharma, *Phys. Rev. C* **84**, 054916 (2011).
 [31] S. Zhang, J. H. Chen, H. Crawford, D. Keane, Y. G. Ma, and Z. B. Xu, *Phys. Lett.* **B684**, 224 (2010).
 [32] G. Chen et al., *Phys. Rev. C* **86**, 054910 (2012).
 [33] G. Chen, H. Chen, J. Wu, D. S. Li, and M. J. Wang, *Phys. Rev. C* **88**, 034908 (2013).
 [34] V. Topor Pop and S. Das Gupta, *Phys. Rev. C* **81**, 054911 (2010).
 [35] J. Steinheimer, K. Gudima, A. Botvina, I. Mishustin, M. Bleicher, and H. Stoecker, *Phys. Lett.* **B714**, 85 (2012).
 [36] S. Chatterjee and B. Mohanty, *Phys. Rev. C* **90**, 034908 (2014).
 [37] S. Chatterjee, B. Mohanty, and R. Singh, *Phys. Rev. C* **92**, 024917 (2015).
 [38] C. B. Dover, U. Heinz, and E. Schnedermann, *Phys. Rev. C* **44**, 1636 (1991).
 [39] F. Retière and M. A. Lisa, *Phys. Rev. C* **70**, 044907 (2004).
 [40] R. Mattiello, H. Sorge, H. Stoecker, and W. Greiner, *Phys. Rev. C* **55**, 1443 (1997).
 [41] L. W. Chen, C. M. Ko, and B. A. Li, *Phys. Rev. C* **68**, 017601 (2003); *Nucl. Phys. A* **729**, 809 (2003); *Phys. Rev. C* **69**, 054606 (2004).
 [42] L. W. Chen and C. M. Ko, *Phys. Rev. C* **73**, 044903 (2006).
 [43] Y. Oh, Z. W. Lin, and C. M. Ko, *Phys. Rev. C* **80**, 064902 (2009).
 [44] F. Cooper and G. Frye, *Phys. Rev. D* **10**, 186 (1974).
 [45] R. Scheibl and U. Heinz, *Phys. Rev. C* **59**, 1585 (1999).
 [46] J. D. Bjorken, *Phys. Rev. D* **27**, 140(1983).
 [47] L. W. Chen, V. Greco, C. M. Ko, S. H. Lee, and W. Liu, *Phys. Lett.* **B601**, 34 (2004); L. W. Chen, C. M. Ko, W. Liu, and M. Nielsen, *Phys. Rev. C* **76**, 014906 (2007).
 [48] S. S. Adler et al. (The PHENIX Collaboration), *Phys. Rev. C* **69**, 034909 (2004).
 [49] B. I. Abelev et al. (The STAR Collaboration), arXiv:0909.0566 [nucl-ex].
 [50] G. Ropke, *Phys. Rev. C* **79**, 014002 (2009).
 [51] I. Tanihata et al., *Phys. Rev. Lett.* **55**, 2676 (1985).
 [52] M. Wang et al., *Chin. Phys. C* **36**, 1603 (2012).
 [53] G. Audi et al., *Chin. Phys. C* **36**, 1157 (2012).
 [54] J. Adams et al. (The STAR Collaboration), *Phys. Rev. Lett.* **92**, 112301 (2004).
 [55] P. Danielewicz and G. F. Bertsch, *Nucl. Phys. A* **533**, 712

(1991); P. Danielewicz, Nucl. Phys. **A545**, 21c (1992); P. Danielewicz and Q. Pan, Phys. Rev. C **46**, 2002 (1992).